Journal of Power Sources 196 (2011) 4729–4734

Contents lists available at ScienceDirect

Journal of Power Sources

journal homepage: www.elsevier.com/locate/jpowsour

A precious-metal free micro fuel cell accumulator

C. Bretthauer*, C. Müller, H. Reinecke

University of Freiburg-IMTEK, Department of Microsystems Engineering, Laboratory for Process Technology, Georges-Köhler-Allee 103, 79110 Freiburg, Germany

ARTICLE INFO

Article history:
Received 16 November 2010
Received in revised form 5 January 2011
Accepted 17 January 2011
Available online 26 January 2011

Keywords:
Micro fuel cell
Fuel cell accumulator
Hydride air accumulator
Micro energy harvesting
Alkaline polymer electrolyte fuel cell
Non precious-metal catalyst

ABSTRACT

In recent years, integrated fuel cell (FC) type primary and secondary batteries attracted a great deal of attention as integrated on-chip power sources due to their high theoretical power densities. Unfortunately, the costs of these devices have been rather high. This is partially due to the involved clean-room processes, but also due to the fact that these devices generally rely on expensive precious-metals such as Pd and Pt. Therefore we developed a novel integrated FC type accumulator that is based on non-precious-metals only. The key component of the presented accumulator is its alkaline polymer electrolyte membrane that allows not only the usage of a low-cost AB_5 type hydrogen storage electrode, but also the usage of $La_{0.6}Ca_{0.4}CoO_3$ as a precious-metal free bifunctional catalyst for the air-breathing electrode. Additionally the presented design requires only comparatively few cleanroom processes which further reduces the overall production costs. Although abdicating precious-metals, the presented accumulator shows an open circuit voltage of 0.81 V and a maximum power density of 0.66 mW cm^{-2} which is comparable or even superior to former precious-metal based cells.

1. Introduction

Modern microelectronics are not only continuously shrinking they also consume less and less power. Against this background one may have the vision of an autonomous microsystem, carrying its own long-lasting power supply. Unfortunately, as system size decreases, less and less space is available for integrated batteries as well, and even more important, the amount of stored energy will always be finite. There are however many applications where an extended lifetime is virtually crucial for their functionality and success, e.g. in case of limited accessibility, such as tire pressure sensors or biomedical implants. The ultimate on-chip power supply should therefore be a self-renewing energy source. This strategy of a self-renewing micro power supply is pursued by the concept of micro energy harvesting (MEH). In an MEH system a micro generator converts ambient energy to electrical energy to power an application. Unfortunately it is not guaranteed, that the ambient energy level will be always high enough to provide sufficient power to the system as harvested energy usually manifests itself in rather irregular, random and low-energy bursts. Therefore excess energy of the harvester needs to be stored in order to reconcile periods of very low ambient power. Thus, integrated energy storage devices are still very important even when an MEH based approach is pursued.

One appealing form of integrated energy storage is H_2/air, or so called fuel cell type batteries, as these devices promise very high volumetric energy densities of more than 2000 Wh l^{-1}. Consequently, this type of battery has recently attracted more and more attention and primary [1–3] as well as secondary type cells have been realized [4,5]. However, a mayor issue of these devices is their high production cost. Thereby the costs originate on the one hand from the expensive cleanroom manufacture, and on the other hand from the expensive hydrogen storage and catalyst materials.

Therefore the aim of this work is the development of a less cost intensive FC type accumulator that uses non-precious-metals only and requires only few cleanroom processing steps. Unlike the devices presented in [1–4] that all relied on a proton exchange membrane (PEM), the new accumulator follows the idea of [5] by using an alkali anion exchange membrane (AAEM) to separate the anode from the cathode. This change in pH allows both, the usage of a standard AB_5 type hydrogen storage and a precious-metal free bifunctional oxygen catalyst ($La_{0.6}Ca_{0.4}CoO_3$), instead of platinum as it was done in Ref. [5].

2. Experimental

2.1. Design and working principle

Fig. 1 shows a schematic cross section of the new cell type. It consists of an air-breathing electrode III and an AB_5 type hydrogen storage electrode VI, both separated by an anionic conducting polymer electrolyte membrane II. The accumulator is integrated in a silicon substrate IV including Si_3N_4 diffusion barriers IX for the ions as well as for the stored hydrogen. The liquid alkaline electrolyte is distributed over the porous MH storage and an additional

* Corresponding author. Tel.: +49 7612037250; fax: +49 7612037352.
E-mail address: bretthau@imtek.de (C. Bretthauer).

0378-7753/$ – see front matter © 2011 Elsevier B.V. All rights reserved.
doi:10.1016/j.jpowsour.2011.01.067

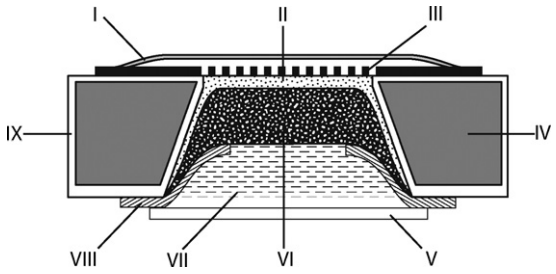

Fig. 1. Principle design of the integrated MH/air accumulator with gas permeable membrane I, polymer electrolyte II, air-breathing electrode III, substrate IV, lid V, MH storage VI, electrolyte reservoir VII, current collector VIII and diffusion barrier IX.

reservoir VII. This not only guarantees that the polymer electrolyte is always humid enough to develop high ionic conductivity but also that every part of the storage and the air-breathing electrode can be electrochemically active for charging or discharging. On the backside, the storage is connected by a sputtered thin film current collector VIII and the cell is sealed by a lid VII. The front of the cell is covered by a gas permeable but water repellent PTFE membrane to prevent the cell from drying out. The working principle of the cell is as follows: during the charging process water is reduced at the AB_5 hydrogen storage to form metal hydride (MH) and hydroxyl ions, whereas at the air-breathing electrode hydroxyl ions from the polymer electrolyte are oxidized to oxygen and water. During the discharge process hydrogen, stored as MH, is oxidized by reacting with hydroxyl ions from the aqueous electrolyte, whereas at the cathode oxygen from the air is reduced to hydroxyl ions. Thereby the produced water is recollected at the hydrogen storage where it can be used for later recharge. The reaction equations are thus

$$4OH^- \rightleftharpoons 2H_2O + O_2 + 4e^- \quad (1)$$

for the air-breathing electrode and

$$4H_2O + 4e^- \rightleftharpoons 4H(\text{as}\,MeH_x) + 4OH^- \quad (2)$$

for the metal hydride electrode. Consequently, the theoretical maximum achievable voltage is 1.23 V as with a hydrogen/oxygen fuel cell.

2.1.1. The polymer electrolyte

As mentioned above, a polymer electrolyte is used to separate the anode from the cathode. In conventional PEMFCs and also in most integrated fuel cells [1–4] the polymer electrolyte is of acidic nature. This type of polymer electrolyte is not suited to be used in combination with AB_5 metal hydrides, as these alloys are unstable in acidic environment. Additionally, the low pH makes high demands on the used catalyst materials in terms of chemical stability. Hence, expensive precious-metal catalysts like Pt or Ru are still the catalyst materials of choice for PEMFCs and account for a large part of the total FC costs. These restrictions can be overcome by using an alkaline polymer electrolyte since electrode kinetics at the anode and cathode are much more facile at high pH and therefore cheaper non-precious catalyst and hydrogen storage materials can be used as well [5,6]. Additionally, another typical PEMFC problem is inherently eliminated. During the operation of a PEMFC, the reaction water is produced at the cathode. If this water is not removed quickly enough, a closed thin film of water will eventually inhibit further oxygen access to catalytically active sites, leading to severe voltage and power losses. This effect is generally known as flooding. In alkaline media on the other hand, reaction water is produced at the anode side, as can be seen from Eq. (2). Here flooding is not a problem as the electrode is immersed in aqueous electrolyte anyway. In fact, water production at the metal hydride electrode is even desired, since the recollected water is essential for later recharge. However, the main problem of alkaline polymer electrolytes remains their bad availability and low ionic conductivity. Unlike proton conducting polymers like Nafion, anionic conducting polymer electrolytes have been far less in the focus of research and at present there are only few commercial polymer electrolytes available. Consequently, the conductivity and chemical stability of the few materials available is not so highly developed as for their acidic counterparts. In this work A3 Polymer Electrolyte (A3PE), an ionomer solution developed by TOKUYAMA, was used as the electrolyte which is chemically stable in alkaline solution up to a temperature of 70 °C. The active part of this ionomer is a quarternary ammonium group and the ionic conductivity of the polymer in 1 M KOH, determined by electrochemical impedance spectroscopy, is 3 mS cm^{-1} which is about two orders of magnitude less than the conductivity of Nafion.

2.1.2. The metal hydride electrode

Generally speaking metal hydrides are compounds of metals or alloys with hydrogen whereby the hydrogen atoms occupy interstitial sites in the host crystal lattice and can be understood as a solution of atomic hydrogen within a metal or alloy. The amount of absorbed hydrogen within the metal is a function of temperature and pressure. With increasing hydrogen pressure more hydrogen is able to enter the metal. Increasing temperature on the other hand leads to a higher hydrogen desorption pressure and thereby reduces the hydrogen content. The relation between hydride formation, temperature and pressure is captured in pressure composition isotherms (PCI) which generally show a wide plateau region in which the desorption pressure rises only slightly with increasing hydrogen content. For a self-breathing accumulator it is essential that this plateau pressure is as low as possible and particularly it has to be below atmospheric pressure for the entire operating temperature. Otherwise the metal hydride will release hydrogen not only by diffusion but also due to hydrogen overpressure, leading to unacceptably high self discharge rates. In this work AUERSTORE® AB_5, a $LaNi_5$ based hydrogen storage alloy by TREIBACHER, was used as the storage material as it shows a subatmospheric hydrogen desorption pressure plateau up to an operating temperature of 60 °C [5]. The capacity, specified by TREIBACHER, is greater than 290 mAh g^{-1} or 1576 mAh cm^{-3}. The hydride material was ground to a mean particle size of 6 μm and mixed with a solution of A3PE as binder in a ratio of 15:1 by weight. The resulting blend can be dried and results in a conductive but porous MH storage electrode.

2.1.3. The air-breathing electrode

There are more or less three major challenges in the development of a catalyst for the air-breathing electrode. First of all the catalyst has to show good bifunctional catalytic activity. Additionally, it has to be stable against oxidation or other degradation mechanisms. Finally the structure of the catalyst is of paramount importance as it has to provide a high amount of triple phase boundary (TPB) at a high electrical conductivity. According to several groups [7–9] $La_{0.6}Ca_{0.4}CoO_3$ is a stable and powerful bifunctional catalyst for alkaline air electrodes using aqueous alkaline electrolytes such as NaOH or KOH. However, it has never been used in combination with a polymer electrolyte membrane and was therefore tested in combination with A3PE. First $La_{0.6}Ca_{0.4}CoO_3$ was synthesized by citric acid precursor method as described in [7] and characterized by X-ray diffraction. The diffraction pattern of the catalyst, shown in Fig. 2, is in good agreement with data from the International Centre for Diffraction Data (ICDD) reported by Y. Ohno from the Electrotechnical Laboratory, Umezono, Sakura-Mura, Niihari-Gun, Ibaraki, Japan.

Subsequently the catalyst was ground in an agate mortar and mixed with carbon black (Printex L by Degussa) in a ratio of

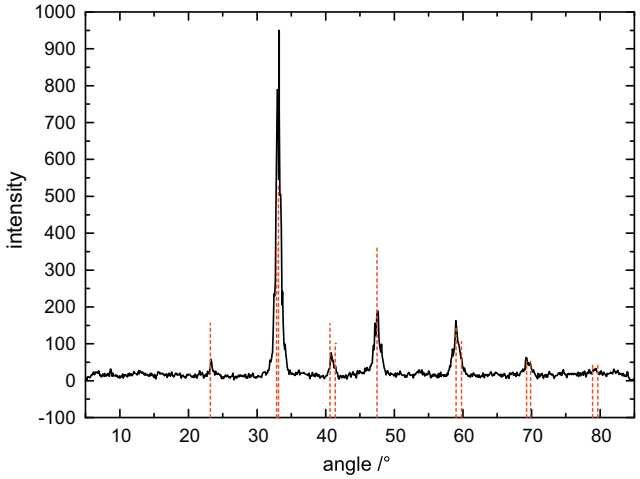

Fig. 2. X-ray diffraction on $La_{0.6}Ca_{0.4}CoO_3$ powder and corresponding peak position data (red dashed) reported by Y. Ohno from the Electrotechnical Laboratory, Umezono, Sakura-Mura, Niihari-Gun, Ibaraki, Japan. (For interpretation of the references to color in this figure legend, the reader is referred to the web version of the article.)

1:4 by weight. The obtained powder was dispersed in a 1 wt.% solution of A3PE. The fraction of A3PE referred to the catalyst/carbon powder was 20 wt.%. The resulting ink was spray coated on a polymer electrolyte supported perforated Ni membrane. A schematic cross section of this electrode is shown in Fig. 3. The resulting average thickness of the catalyst layer was 10 μm with an out-of-plane resistivity of 1500 Ω cm. To measure the performance of the catalyst, linear voltammetry with a scanning speed of 1 mV s^{-1} was performed on electrodes with and without catalyst. The measurement setup is explained in more detail in [5]. Fig. 4 shows the performance change due to the catalyst.

As can be seen, the equilibrium potential of 58 mV versus NHE is the same for both cases. This rather low value suggests that oxygen is mainly reduced by indirect reduction via

$$O_2 + 2H_2O + 2e^- \rightleftharpoons HO_2^- + OH^- \quad (3)$$

$$HO_2^- + H_2O + 2e^- \rightleftharpoons 3OH^- \quad (4)$$

which has also been found by Hermann et al. in [10]. It is also a clearly non-reversible electrode as the onset of oxygen evolution is shifted by 0.55 V from the equilibrium potential. However, the polarization behavior of the catalyst enhanced electrode is obviously superior to the electrode without catalyst. At a cathodic potential of −0.2 V versus NHE the catalyst coated electrode delivers a discharge current density of 2.75 mA cm^{-2} which is 25 times more than the untreated electrode with a current density of 0.11 mA cm^{-2}. Also in anodic direction the catalyst coated electrode performs better; e.g. at 0.85 V versus NHE it shows a factor 7.6 greater current density of 0.76 mA cm^{-2} instead of 0.1 mA cm^{-2}. It

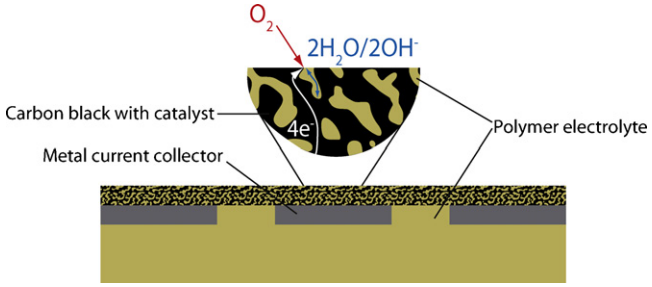

Fig. 3. Schematic cross section of an air-breathing electrode.

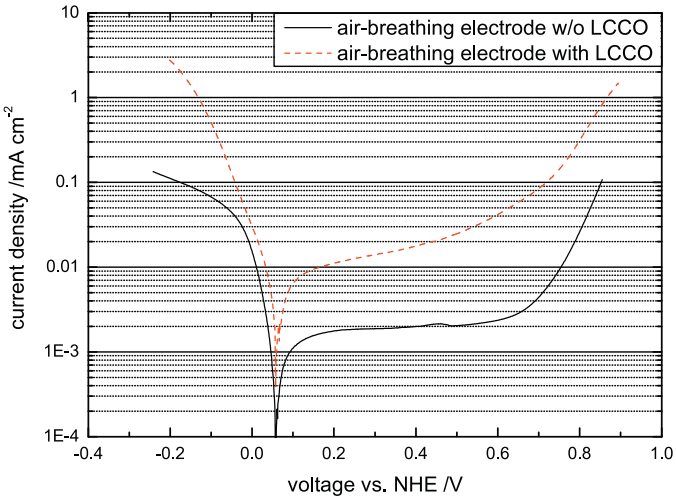

Fig. 4. Linear voltammetry on an air-breathing electrode with and without $La_{0.6}Ca_{0.4}CoO_3$ catalyst at a scanning speed of 1 mV s^{-1}.

can thus be concluded that $La_{0.6}Ca_{0.4}CoO_3$ is also capable to be used in combination with alkaline polymer electrolyte membranes.

2.1.4. Cell manufacture

Fig. 5 shows the entire process flow of cell manufacture, starting with a Si_3N_4 coated silicon wafer. In process step A, an AZ laquer is structured by photo-lithography to define the geometry of the air-breathing electrode. The design consists of a 2 mm × 2 mm membrane with circular perforations of 40 μm diameter with a pitch of 120 μm. In process step B, a nickel layer of 300 nm is sputter deposited and structured via lift-off technique. Subsequently, in process step C, backside lithography is performed and the nitride coating is opened by reactive ion etching (RIE). Additionally the front side is covered by a PMMA protection layer in order to stabilize the membrane during the following KOH etch D. After stripping the PMMA protection layer in acetone, a 1 μm plasma enhanced chemical vapour deposition (PECVD) Si_3N_4 layer is deposited on the entire backside in process step E, including the side walls of the cavity. In the following step F, the nitride layer at the bottom of the cavity is opened by RIE using a silicon shadow mask. At this state, G, the air-breathing electrode is exposed from its backside permitting to dispense a 5 wt.% solution of A3PE. The solution is dried at 60 °C to form a closed 10 μm thick membrane which is then coated by airbrushing the $La_{0.6}Ca_{0.4}CoO_3$ catalyst ink in step H. In a next step, I, the metal hydride storage is deposited in the cavity by dispensing the AB_5/A3PE blend which is again dried at 60 °C. In step J a current collector is sputter deposited using a shadow mask. Finally, the cell is filled with aqueous electrolyte, covered with a lid on the backside and a gas permeable but water repellent 6 μm thick PTFE membrane on the front. Fig. 6 shows a picture of a silicon chip containing four single cells (left) and a cross section of a cell taken by SEM (right).

3. Results and discussion

Fig. 7 shows the cell's discharge characteristics, i.e. current density versus cell voltage and power density, after charging it at 1 mA cm^{-2} for 1 h. As can be seen, the accumulator showed an open circuit voltage V_{ocv} of 0.81 V with an initial activation overvoltage loss of 0.16 V at a current density of 0.2 mA cm^{-2}. Thereafter the IV-characteristic is dominated by Ohmic losses and drops at a constant rate of 127 Ω cm^2 and reaches its maximum power point (MPP) of 0.66 mW cm^{-2} at a voltage of 0.31 V. Comparing this result to key data of similar integrated fuel cell batteries, as shown in Table 1, it

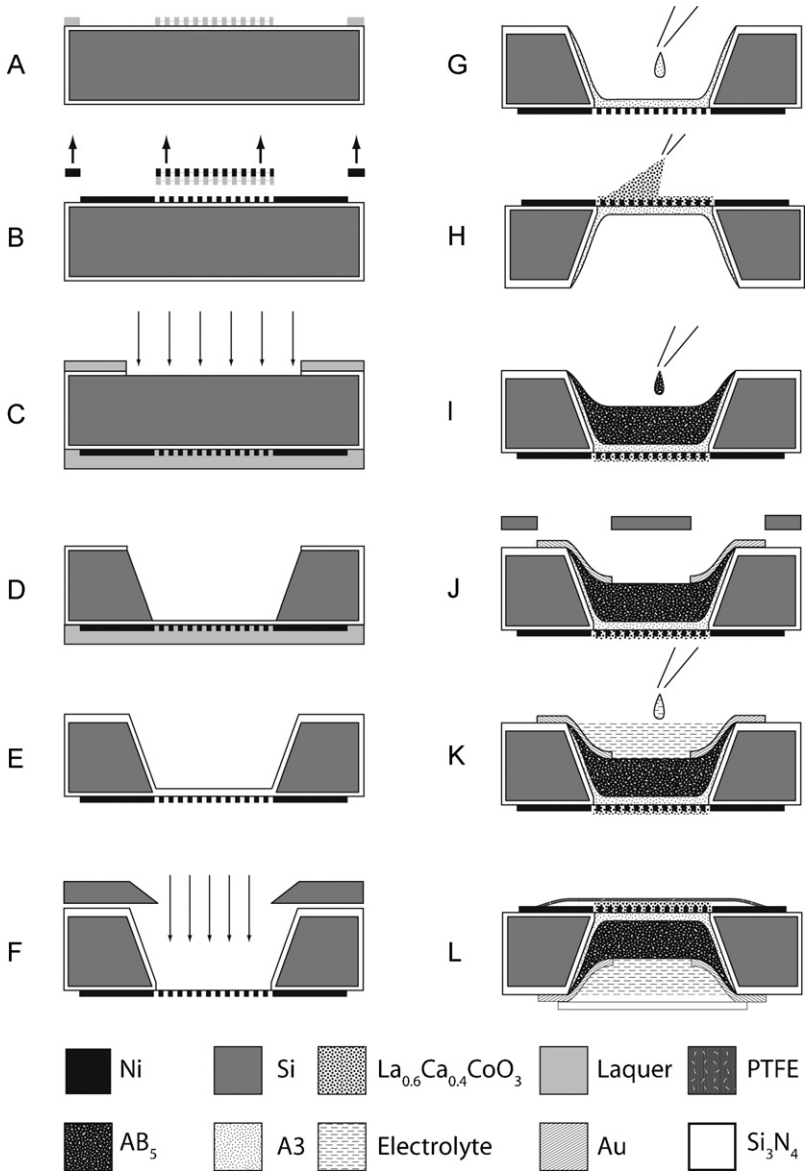

Fig. 5. Cell manufacture with lithography A, sputter deposition and lift-off B, lithography, RIE and protection laquer C, KOH etch D, PECVD-Si_3N_4 deposition E, RIE etch F with Si shadow mask, dispensing of A3PE G, catalyst coating H, dispensing of AB5 hydrogen storage I, metal sputter deposition J with shadow mask, filling with electrolyte K, Si_3N_4 backside capping and front side bonding of PTFE membrane L.

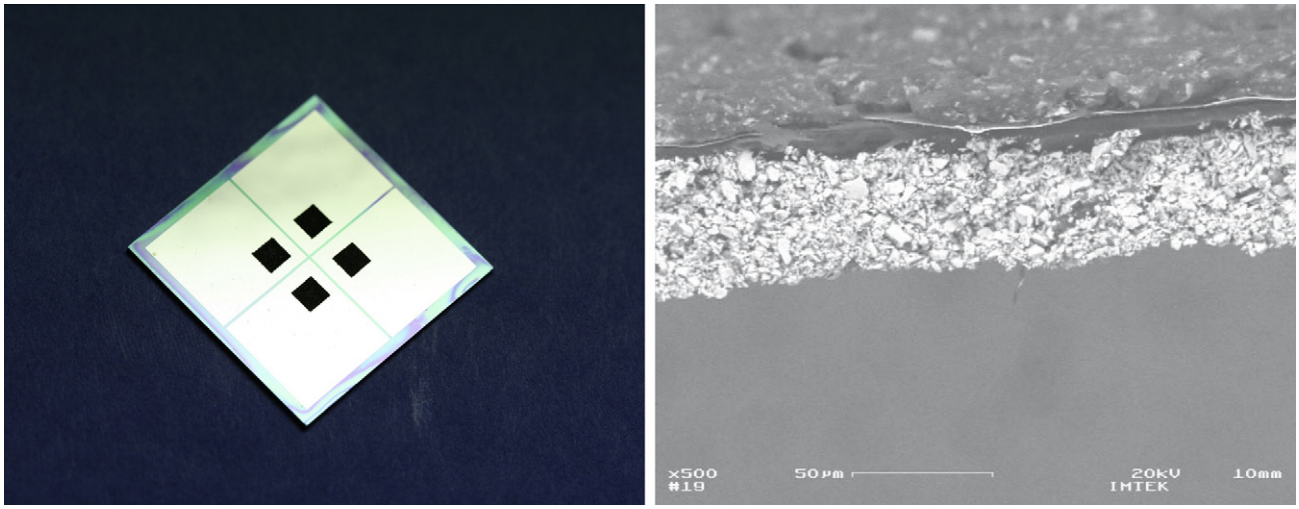

Fig. 6. Four 2 mm × 2 mm cells with $La_{0.6}Ca_{0.4}CoO_3$ catalyst coating on a 19 mm × 19 mm silicon substrate (left). SEM, cross section of a cell (right).

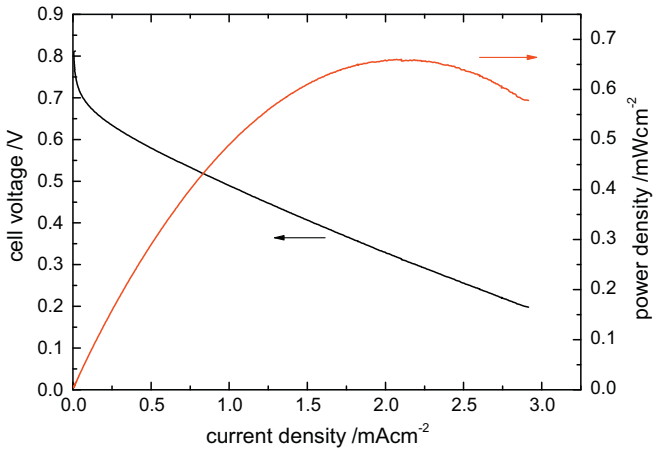

Fig. 7. Discharge performance of a cell, recorded by linear voltammetry at a scanning speed of 1 mV s^{-1}.

Table 1
Key data of similar integrated micro fuel cell batteries.

Anode	Cathode	V_{ocv} (V)	MPP ($mW\,cm^{-2}$)	Cell type	Reference
Pd	Pt	0.7	–	Primary	[1]
Pd	Pt	0.75	0.3	Primary	[2]
$LiAlH_4$	Pt	0.9	1	Primary	[3]
Pd	Pt	0.9	(0.4)	Secondary	[4]
AB_5	Pt	0.88	0.559	Secondary	[5]

can be seen, that the precious-metal free micro accumulator is in deed comparable or even superior in terms of voltage and power density.

In order to characterize the charge–discharge behavior, the cell was repeatedly charged at 1 mA cm^{-2} for 1 h and discharged at discharge current densities of 2–0.5 mA cm^{-2}. The result of these measurements is shown in Fig. 8. It was found that the discharge potentials are very stable until a high degree of discharge and the Faradayic efficiency of the cells is close to 100% for all current densities. This is also in good agreement with experiments on pure AB_5 electrodes which indicated very low self-discharge of the metal hydride.

If the accumulator is meant to be used with energy harvesting devices it is further important to evaluate the cell's voltage

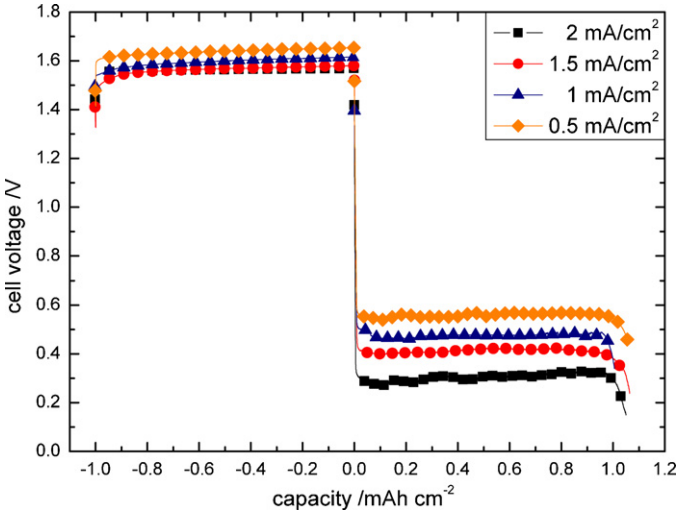

Fig. 8. Charge–discharge cycles at charging current densities of 1 mA cm^{-2} and discharging current densities of 0.5–2 mA cm^{-2}.

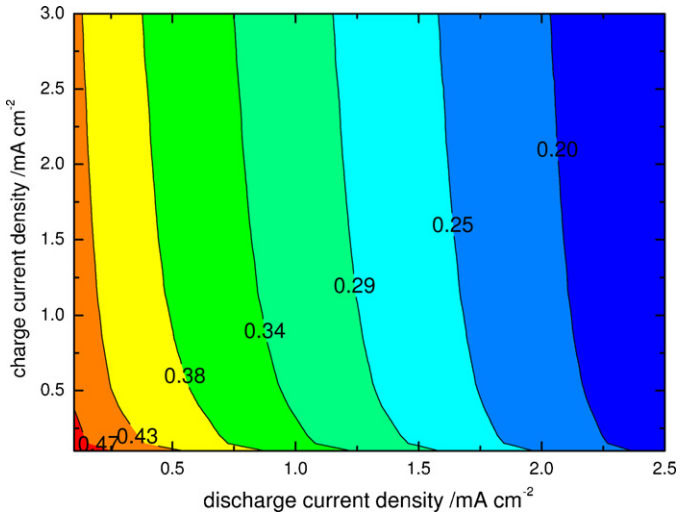

Fig. 9. Voltage efficiency as a function of charge and discharge current density.

efficiency which is defined as the ratio of charging to discharging voltage for a given pair of charging and discharging current densities. It is needless to say that the voltage efficiency increases with decreasing charging and discharging current densities. However, voltage efficiency is not meaningful for vanishing current densities which is why in Fig. 9 a minimum reasonable current density was set to 0.1 mA cm^{-2} both in charge and discharge direction. It was found that at these low current densities a maximum efficiency of 52% can be reached. At the MPP on the other hand the maximum efficiency drops to 23% for a charging current density of 0.1 mA cm^{-2} but stays relatively stable such that at 1.4 mA cm^{-2} it is still at 20%. The reason why the efficiency η_v is restricted to <52% can be ascribed to the polarization behavior of the air-breathing electrode. From Fig. 4 it can be considered that the overpotentials in charge and discharge direction, $\Delta\phi_{chg}$ and $\Delta\phi_{dis}$, for a current density of 0.1 mA cm^{-2} are 0.65 V and −0.05 V, respectively. Further neglecting the comparatively low polarization behavior of the AB_5 electrode, it is straight forward to approximate an upper limit for the voltage efficiency at 0.1 mA cm^{-2} by

$$\eta_v = \frac{V_{dis}(0.1\,mA/cm^2)}{V_{chg}(0.1\,mA/cm^2)} \approx \frac{V_{ocv} - \Delta\phi_{dis}(0.1\,mA/cm^2)}{V_{ocv} + \Delta\phi_{chg}(0.1\,mA/cm^2)} = \frac{0.81\,V - 0.05\,V}{0.81\,V + 0.65\,V} = 0.52 \quad (5)$$

This shows that the air-breathing electrode is essentially limiting the maximum achievable voltage efficiency. Since voltage efficiency is a key parameter for the usage within micro energy harvesting systems, it will be necessary to further improve the catalytic properties of the air-breathing electrode for charge and discharge.

Further comparing the above results to data collected by Patil et al. in a review article from 2008 [11] about lithium based thin film secondary batteries, which is shown in Table 2, it can be seen that the integrated MH/air accumulator is on a competitive or even superior basis in terms of power density and capacity per unit area. The rather low capacity of Li based devices is due to the strong volume change during charging and discharging which leads to manufacturing and stability issues, i.e. the film thickness of the electrodes is only a few μm which annihilates the advantage of their very high energy density storage materials [11].

Unfortunately there is no detailed data available regarding the voltage efficiency of these devices. However, from some of the provided charge–discharge plots it is possible to estimate voltage efficiencies in the range of 70–80%. Realistically seen this will also

Table 2
Performance data of integrated thin film Li batteries [11].

Voltage (V)	Current density ($\mu A\,cm^{-2}$)	Capacity ($\mu Ah\,cm^{-2}$)	Reference
2.5	16	45–150	[12]
3.5–3.6	10	6	[13]
2.8	20	60	[14]
4.2–3.5	1–5	130	[15]
2.7–1.5	10–200	4–10	[16]
2.6–3	5–100	56	[17]

be about the maximum achievable range for the fuel cell accumulator as even with a strongly improved air-breathing electrode there will remain significant overpotential losses due to the complex and slow kinetics of oxygen electrodes in general.

3.1. Conclusion and outlook

A novel, precious-metal free alkaline micro accumulator has been presented with the aim to reduce the overall costs of similar previous systems [1–5]. A comparatively simple cleanroom fabrication process was developed to integrate the accumulator in silicon substrates, so as to enable high integration density. Additionally, it was taken advantage of the cell's high pH by using both an inexpensive AB_5 metal hydride storage and a bidirectional all base metal oxide catalyst, $La_{0.6}Ca_{0.4}CoO_3$, for the air-breathing electrode. First devices were manufactured and characterized. It could be shown that the voltage and power density of the accumulator of 0.81 V and 0.66 $mW\,cm^{-2}$ respectively, are comparable or even superior to similar devices that all rely on Pt air-breathing electrodes due to the acidic nature of the used electrolyte [1–4]. However, the air-breathing electrode was identified to mainly limit the voltage efficiency of the cell which is problematic for applications with MEH devices. Therefore the catalyst ink and spray coating technique have to be further optimized in order to improve the polarization of the air-breathing electrode and minimize overvoltage losses. Furthermore it is envisioned to transfer the design to polymer substrates in order to avoid expensive cleanroom processes at all.

References

[1] G. Erdler, M. Frank, M. Lehmann, H. Reinecke, C. Müller, Sensors and Actuators A (2006) 331–336.
[2] M. Frank, M. Kuhl, G. Erdler, I. Freund, Y. Manoli, C. Müller, H. Reinecke, IEEE Journal of Solid-State Circuits 45 (1) (2010) 205–213.
[3] S. Moghaddam, E. Pengwang, K.Y. Lin, R.I. Masel, M.A. Shannon, Journal of Microelectromechanical Systems 17 (6) (2008) 1388–1395.
[4] M. Frank, G. Erdler, H.-P. Frerichs, C. Müller, H. Reinecke, Journal of Power Sources 181 (2) (2008) 371–377.
[5] C. Bretthauer, C. Müller, H. Reinecke, Electrochimica Acta 54 (25) (2009) 6094–6098.
[6] J.R. Varcoe, R.C.T. Slade, Fuel Cells 5 (2005) 187–200.
[7] S. Müller, K. Striebel, O. Haas., Electrochimica Acta 39 (11–12) (1994) 1661–1668.
[8] D. Chartouni, N. Kuriyama, T. Kiyobayashi, J. Chen, Journal of Alloys and Compounds 330 (2002) 766–770.
[9] M. Bursell, M. Pirjamali, Y. Kiros, Electrochimica Acta 47 (10) (2002) 1651–1660.
[10] V. Hermann, D. Dutriat, S. Müller, C. Comninellis, Electrochimica Acta 46 (2–3) (2000) 365–372.
[11] A. Patil, V. Patil, D. Wook Shin, J.-W. Choi, D.-S. Paik, S.-J. Yoon, Material Research Bulletin 43 (8–9) (2008) 1913–1942.
[12] K. Kanehori, K. Matsumoto, K. Miyauchi, T. Kudo, Solid State Ionics 9 (1983) 1445–1448.
[13] M. Baba, N. Kumagai, H. Kobayashi, O. Nakano, K. Nishidate, Electrochemical and Solid-State Letters 2 (1999) 320.
[14] H. Ohtsuka, S. Okada, J. Yamaki, Solid State Ionics 40 (1990) 964–966.
[15] B.J. Neudecker, N.J. Dudney, J.B. Bates, Journal of the Electrochemical Society 147 (2) (2000) 517–523.
[16] S.D. Jones, J.R. Akridge, Solid State Ionics 53 (1992) 628–634.
[17] G.F. Ortiza, I. Hanzu, P. Knauth, P. Lavel, J.L. Tirado, T. Djenizian, Electrochimica Acta 54 (2009) 4262–4268.